

# Decay Spectroscopy Using the HRIBF Recoil Mass Spectrometer

C. J. Gross<sup>1,2,\*</sup>, T. N. Ginter<sup>3</sup>, J. J. Ressler<sup>4</sup>, J. C. Batchelder<sup>1</sup>, R. Grzywacz<sup>5</sup>, A. Piechaczek<sup>6</sup>, W. B. Walters<sup>4</sup>, M. Wiescher<sup>7</sup>, K. Rykaczewski<sup>2</sup>, A. Aprahamian<sup>7</sup>, C. R. Bingham<sup>2,5</sup>, Z. Janas<sup>8</sup>, B. D. MacDonald<sup>9</sup>, E. F. Zganjar<sup>6</sup>

<sup>1</sup>*Oak Ridge Institute for Science and Education, Oak Ridge, Tennessee 37831 USA*

<sup>2</sup>*Physics Division, Oak Ridge National Laboratory, Oak Ridge, Tennessee 37831 USA*

<sup>3</sup>*Department of Physics and Astronomy, Vanderbilt University, Nashville, TN 37235 USA*

<sup>4</sup>*Department of Chemistry, University of Maryland, College Park, Maryland 20742, USA*

<sup>5</sup>*Department of Physics and Astronomy, University of Tennessee, Knoxville, TN 37996, USA*

<sup>6</sup>*Department of Physics and Astronomy, Louisiana State University, Baton Rouge, LA 70803, USA*

<sup>7</sup>*Department of Physics, Notre Dame University, Notre Dame, IN 46556, USA*

<sup>8</sup>*Joint Institute for Heavy Ion Research, Oak Ridge, Tennessee 37831 USA*

<sup>9</sup>*School of Physics, Georgia Institute of Technology, Atlanta, GA 30332, USA*

(January 28, 2000)

Two decay spectroscopy experiments performed with the Recoil Mass Spectrometer at the Holifield Radioactive in Beam Facility are described. Utilizing the Moving Tape Collector, the  $\beta^+$  decay half-life of  $^{80}\text{Zr}$  has been measured to be  $4.1^{+0.8}_{-0.6}$  s. The resulting decrease in mass 80 production during the rapid proton capture process, suggests that  $^{80}\text{Zr}$  may not be a significant waiting point and the process may proceed to heavier masses. The observation of proton fine structure is reported for the first time in spherical nuclei. Three new decay branches, apparently from the two previously known states in  $^{146}\text{Tm}$ , have been observed using double-sided silicon strip detectors. Arising from the complex configuration mixing common to odd-odd nuclei, our preliminary results suggest relative energy differences and spins and parities in the  $^{146}\text{Tm}$  parent and  $^{145}\text{Er}$  daughter isotopes.

**KEYWORDS:** Recoil Mass Spectrometer, moving tape collector, proton and beta radioactivity

**PACS:** 23.50.+z, 26.30.+k, 27.60.+j, 27.50.+e

The study of radioactivity from nuclei far from stability is critical to our understanding of nuclei and the world around us. These nuclei provide stringent tests of the predictive power of nuclear models developed from data on nuclei much closer to stability. Lying at the extremes of stability, small changes in energy levels caused by such phenomena as neutron-proton pairing or coupling to neighboring states including those in the continuum, can lead to drastic changes in decay branchings, energies, and half-lives. These effects can influence the rate of nucleosynthesis [1] and can result in valuable probes into the nuclear wavefunction [2].

The nucleosynthesis process in explosive stellar events is governed by capture and decay rates which are, in many cases, unknown. We still do not have a good understanding of how the natural abundances of the lightest stable Mo and Ru are enhanced. These nuclei may be produced through the rapid proton capture process (rp-process) which can occur in X-ray bursts. X-ray bursts are formed when matter from a nearby star is pulled onto a neighboring neutron star. The environments in these phenomena have very high temperatures ( $T \geq 10^9$  K) and proton densities. The rp-process [3], governed by the proton capture rates and  $\beta^+$  decay rates, follows the proton drip line from  $^{56}\text{Ni}$  towards  $^{100}\text{Sn}$ . The progression toward higher masses can be stopped at critical points or waiting points where nuclei with long  $\beta^+$  half-lives are immediately below a proton unstable nucleus. The waiting points allow the temperatures to cool and thus, terminate the process of nucleosynthesis. One possible waiting point is  $^{80}\text{Zr}$  and the proton unstable  $^{81}\text{Nb}$  [4]. We report on the half-life of  $^{80}\text{Zr}$  and its possible implications to the rp-process. This study has also been reported in ref. [5].

The study of nuclei beyond the proton drip line can test nuclear structure models and perhaps detect the effects of coupling to unbound continuum states which would modify the nuclear wave functions. Proton radioactivity studies have been shown [6–9] to provide information on the wavefunctions of the parent state through the "simple WKB" relationship [10] between its angular momentum, decay energy, and half-life. The recent observation [2] in  $^{131}\text{Eu}$  of proton radioactivity with a decay branch to an excited state indicates a mixing of the wavefunction through deformation. We have undertaken a search for multiple proton decay branches in odd-odd, spherical nuclei where complex wavefunctions should exist through the configuration mixing of many low-lying states involving both proton and neutron single-particle states. Such decays populate excited neutron states in the even-Z, odd-N daughter which

---

\*Corresponding author, Tel: +1-865-576-7698; Fax: +1-865-574-1268; email: cgross@mail.phy.ornl.gov

may be difficult to access in any other way [11]. We report on our preliminary results of multiple proton decay branches in the odd-odd nucleus  $^{146}\text{Tm}$ .

Central to these studies is the Recoil Mass Spectrometer (RMS) [12] at the Holifield Radioactive Ion Beam Facility. Through the fast, in-flight separation of the heavy-ion fusion-evaporation reaction products, the RMS provides identification of reaction products through their mass-to-charge ( $A/Q$ ) ratio. With the addition of a momentum separator for beam rejection, the mass analyzer uses a Rochester-type electric-magnetic-electric dipole configuration [13] to separate masses with a resolution of  $M/\Delta M = 400$  and very little background from primary beam. The RMS is shown in fig. 1 and is described in more detail in ref. [12].

## I. THE $^{80}\text{Zr}$ RP-PROCESS WAITING POINT

Zirconium-80 was populated through the reaction  $^{24}\text{Mg}(^{58}\text{Ni},2n)$  at 195 MeV using a  $500\ \mu\text{g}/\text{cm}^2$ , enriched target. Mass 80 recoils of charge state  $24^+$  were transmitted on the central axis of the RMS and implanted into a 35-mm aluminized mylar tape. As part of the Moving Tape Collector [12,14,15], the tape was moved in 30 s intervals (later optimized to 20 s) to bring the activity to a counting station similar to fig 2. The counting station consists of three Clover Ge detectors, a large area, planar Ge detector, and three plastic scintillators in front of the Clovers. Prompt and delayed  $\beta-\gamma$  coincidence data were written to tape. The success of the experiment depended upon the population of the recently reported [16] 312 keV,  $2^+$  isomer in  $^{80}\text{Y}$ . This state decays with a 4  $\mu\text{s}$  half-life via an 84 keV  $\gamma$  ray which can be used as a unique tag of the  $^{80}\text{Zr}$  decay. A low-energy level diagram of the  $^{80}\text{Zr} \rightarrow ^{80}\text{Y}$  decay process is shown in fig. 3a. The resulting delayed- $\gamma$  coincidence spectrum gated by 84 keV is shown in fig. 3b and clearly provides a unique identification of the  $^{80}\text{Zr}$  decay. The decay rate data, consisting of 87 events of which 11 are taken as background, are shown in fig. 3c and result in a half-life of  $4.1_{-0.6}^{+0.8}$  s [5].

The mass 80 energy and abundance results of a one-mass zone model [3] for an X-ray burst incorporating our  $^{80}\text{Zr}$  decay data are shown in fig. 4. Although the difference in energy production is small, the mass 80 isotope abundances are more tightly constrained. The short half-life of  $^{80}\text{Zr}$  and the smaller effective  $^{80}\text{Y}$  half-life (due to  $^{80}\text{Zr}$  feeding the 5 s isomer instead of the 30 s ground state) result in a more rapid transition to heavier masses due to the fast proton capture on  $^{80}\text{Y}$  and  $^{80}\text{Sr}$ . Thus, the formation of  $^{80}\text{Kr}$  in the neutron star where X-ray bursts are found, should be reduced nearly an order of magnitude.

## II. PROTON FINE STRUCTURE IN $^{146}\text{Tm}$

Thulium-146 was populated through the reaction  $^{58}\text{Ni}(^{92}\text{Mo},p3n)$  at 292 MeV using a  $900\ \mu\text{g}/\text{cm}^2$  enriched (96%) target. Mass 146 recoils of charge states  $26^+$  and  $27^+$  were transmitted by the RMS operated in converging mode. After passing through the focal plane's position sensitive avalanche counter (PSAC), the ions were implanted into a 40 strip by 40 strip (40 mm x 40 mm) double-sided silicon strip detector (DSSD) which effectively makes 1600 separate pixels [12,17–19]. Implantation events are determined by coincidences between the DSSD and the PSAC. Decay events are DSSD events not in coincidence with the PSAC. All events are time stamped with a 48-bit counter running at 10 MHz. A schematic illustration of the experimental setup and decay spectrum within 1 s after implantation is shown in fig. 5. The large clusters of peaks at high energies correspond to alpha decays from heavier nuclei produced from the contaminant Mo isotopes in the target and transmitted through the RMS with similar mass-to-charge ratios as the  $A=146$  products. The low energy peaks correspond to the previously known transitions at 1.12 MeV and 1.19 MeV. By setting shorter time constraints between implantation and decay, smaller peaks below the two known transitions can be observed in fig. 6. By setting narrow mass gates on the PSAC spectrum, these transitions can be assigned to  $^{146}\text{Tm}$  and  $^{147}\text{Tm}$  since any contaminant reaction is not expected to produce any unknown proton emitters. The  $^{147}\text{Tm}$  events arise from an inaccurate setting of the mechanical slits which did not fully block the  $A=147$  products. To ensure these events are not an artifact from the known proton and alpha decays which escape the detector and do not deposit all their energy in the detector, we adjusted the implantation depth of the ions by implanting them at approximately 10 and 60 MeV through the use of energy degraders located immediately before the detector. The effect of implantation depth on the background can be observed in fig. 7. In both cases, the peaks remain and are unshifted in energy. Therefore, we assign these proton decays to  $^{146}\text{Tm}$ . Our preliminary results are summarized in table 1 along with WKB proton partial half-life estimates for each transition as a function of the angular momentum barrier.

The active single-particle orbitals in this mass region are  $s_{\frac{1}{2}}$ ,  $d_{\frac{3}{2}}$ , and  $h_{\frac{11}{2}}$  or  $\Delta l$  equals 0, 2, and 5  $\hbar$ . Our results agree with previous studies [20] and indicate that the  $h_{\frac{11}{2}}$  orbital ( $\Delta l = 5$ ) dominates the decay through the 1.120 and 1.191 MeV transitions. Note that  $\beta$  decay is also expected to compete with proton emission in  $^{146,147}\text{Tm}$ . The

branches in the decay arise from components of different angular momentum within the wavefunction. The discussion below assumes the following:

- 1) The states populated in  $^{146}\text{Tm}$  are primarily yrast and decay to two low energy states. The state populated the strongest is the  $\pi h_{\frac{11}{2}} \otimes \nu h_{\frac{11}{2}}$  and the other state is of opposite parity.
- 2) The two observed states in  $^{146}\text{Tm}$  are comprised of a proton and a neutron which are coupled to moderately high spins and contain at least one nucleon in the  $h_{\frac{11}{2}}$  orbital.
- 3) The neutron configuration in  $^{146}\text{Tm}$  when proton emission occurs determines which states in the  $^{145}\text{Er}$  daughter [21] are populated.
- 4) The number of decay branches indicates the minimum number of different proton wavefunctions contributing to the state.

The state with three decay branches seems most straightforward to understand with three similar half-life values near the experimental  $\sim 100$  ms for all three different angular momentum values. Assuming near equal contribution from each orbital, we tentatively assign this state in  $^{146}\text{Tm}$  as  $I^\pi = \mathbf{5,6}^-$  arising from the following components:

$$[\pi(h_{\frac{11}{2}}) \otimes \nu(s_{\frac{1}{2}})]^{5,6-} + [\pi(h_{\frac{11}{2}}) \otimes \nu(d_{\frac{3}{2}})]^{5,6-} +$$

$$[\pi(d_{\frac{3}{2}}) \otimes \nu(h_{\frac{11}{2}})]^{5,6-} + [\pi(s_{\frac{1}{2}}) \otimes \nu(h_{\frac{11}{2}})]^{5,6-}.$$

Our assumptions lead us to assume that one state in  $^{145}\text{Er}$  is based on the high spin  $\nu h_{\frac{11}{2}}$  orbital and should be populated by both proton emitting states. Thus, this state should be populated by the 0.885 ( $\Delta l=0$ ) and 1.120 MeV ( $\Delta l=5$ ) decay branches and has  $I^\pi = \frac{9}{2}, \frac{11}{2}^-$ . This fixes the relative energy separation of the two parent states to 0.235 MeV with the  $I^\pi = \mathbf{5,6}^-$  as the ground state of  $^{146}\text{Tm}$ . The ground state of the  $^{145}\text{Er}$ , populated by the 1.191 MeV proton, should be  $I^\pi = \frac{1}{2}^+$  and lies 0.305 MeV lower in energy than the state populated by both proton-emitting states.

The  $I^\pi = \frac{7}{2}, \frac{9}{2}, \frac{11}{2}^-$  state, populated by the 0.935 MeV proton, lies 0.265 MeV above the ground state. The  $^{146}\text{Tm}$  state with only two decay branches, 1.120 and 1.032 MeV, cannot be a fully aligned configuration since assumptions (3) and (4) would require only one state in the daughter be populated. An assignment of  $I^\pi = 10^+$  state would suggest that both branches decay to the same states as those populated by the 0.885 and 0.935 MeV transitions; energy summation of the different decay branches rule out this possibility. Thus, the most logical conclusion to draw is that this state is the  $I^\pi = \mathbf{9}^+$  arising from the following components:

$$[\pi(h_{\frac{11}{2}}) \otimes \nu(h_{\frac{11}{2}})]^{9+} + [\pi(h_{\frac{11}{2}}) \otimes \nu(h_{\frac{11}{2}})]^{9+}.$$

Thus, the state populated by the 1.035 MeV proton branch has  $I^\pi = \frac{7}{2}, \frac{9}{2}, \frac{11}{2}^-$  and lies at 0.393 MeV. This discussion can be summarized by the decay scheme shown in fig. 8. The spins in bold face indicate those favored by energy level systematics in the  $N=77$  isotones [11] where the  $\frac{11}{2}^-$  state is lowest in energy followed by the  $\frac{9}{2}^-$  and  $\frac{7}{2}^-$ . This is the most extensive proton decay scheme observed to date and provides relative energies of the low-lying states in  $^{146}\text{Tm}$  and  $^{145}\text{Er}$ .

### III. CONCLUSION

We have measured the half-life of  $^{80}\text{Zr}$  to be  $4.1_{-0.6}^{+0.8}$  s. A one-zone mass restricted rp-process calculation suggests that the amount of  $^{80}\text{Kr}$  produced in X-ray bursts is reduced by roughly one order of magnitude. This allows the process to proceed to heavier masses. In addition, we have observed proton fine structure decays in  $^{146}\text{Tm}$  and have identified the most complex proton emitter decay spectrum studied to date. The decay pattern indicates the wavefunctions of the parent are complex and yet, through a simple WKB analysis, relative energies, spins, and parities are suggested for states in the parent and the daughter.

### IV. ACKNOWLEDGEMENTS

We thank the staff of the HRIBF for their hard work in providing the beams and support for these experiments. Oak Ridge National Laboratory (ORNL) is managed by Lockheed Martin Energy Research Corp. for the U.S. Department of Energy (DOE) under contract DE-AC05-96OR22464. This research was also supported by DOE and the National Science Foundation through contract numbers DE-FG02-96ER40978 (Louisiana State University), DE-AC05-76OR00033 (Oak Ridge Institute for Science and Education), DE-FG02-96ER40963 (University of Tennessee), DE-FG05-87ER40407 (Vanderbilt University), DE-FG02-94ER40834 (University of Maryland), PHY99-01133 (Notre

- [1] H. Schatz, A. Aprahamian, J. Gořres, M. Wiescher, T. Rauscher, J. F. Rembges, F.-K. Thielemann, B. Pfeiffer, P. Möller, K.-L. Kratz, H. Herndl, B. A. Brown, and H. Rebel, *Phys. Rep.* **294** (1998) 167.
- [2] A. A. Sonzogni, C. N. Davids, P. J. Woods, D. Seweryniak, M. P. Carpenter, J. J. Ressler, J. Schwartz, J. Uusitalo, and W. B. Walters, *Phys. Rev. Lett.* **83** (1999) 1116.
- [3] M. Wiescher, J. Gorres, and H. Schatz, *Phil. Trans. Roy. Soc.* **356** (1998) 1949 and references therein.
- [4] Z. Janas, C. Chandler, B. Blank, P. H. Regan, A. M. Bruce, W. N. Catford, N. Curtis, S. Czajkowski, Ph. Dessagne, A. Fleury, W. Gelletly, J. Giovinazzo, R. Grzywacz, M. Lewitowicz, C. Longour, C. Marchand, Ch. Mieke, N. A. Orr, R. D. Page, C. J. Pearson, M. S. Pravikoff, A. T. Reed, M. G. Saint-Laurent, J. A. Sheikh, S. M. Vincent, R. Wadsworth, D. D. Warner, and J. S. Winfield, *Phys. Rev. Lett.* **82** (1999) 295.
- [5] J. J. Ressler, A. Piechaczek, W. B. Walters, A. Aprahamian, M. Wiescher, J. C. Batchelder, C. R. Bingham, D. S. Brenner, T. N. Ginter, C. J. Gross, R. Grzywacz, D. Kulp, B. MacDonald, W. Reviol, J. Rikowska, K. Rykaczewski, J. A. Winger, and E. F. Zganjar, *Phys. Rev. Lett.*, in press.
- [6] P. J. Woods and C. N. Davids, *Annu. Rev. Nucl. Part. Sci.*, **47**, (1997) 541 and references therein.
- [7] J. C. Batchelder, C. R. Bingham, K. Rykaczewski, K. S. Toth, T. Davinson, J. A. McKenzie, P. J. Woods, T. N. Ginter, C. J. Gross, J. W. McConnell, E. F. Zganjar, J. H. Hamilton, W. B. Walters, C. Baktash, J. Greene, J. F. Mas, W. T. Milner, S. D. Paul, D. Shapira, X. J. Xu, and C. H. Yu *Phys. Rev. C* **57** (1998) R1042.
- [8] C. R. Bingham, J. C. Batchelder, K. Rykaczewski, K. S. Toth, C.-H. Yu, T. N. Ginter, C. J. Gross, R. Grzywacz, M. Karny, S. H. Kim, B. D. MacDonald, J. Mas, J. W. McConnell, P. B. Semmes, J. Szerypo, W. Weintraub, and E. F. Zganjar, *Phys. Rev. C*, **59**, (1999) R2984.
- [9] K. Rykaczewski, J. C. Batchelder, C. R. Bingham, T. Davinson, T. N. Ginter, C. J. Gross, R. Grzywacz, M. Karny, B. D. MacDonald, J. F. Mas, J. W. McConnell, A. Piechaczek, R. C. Slinger, K. S. Toth, W. B. Walters, P. J. Woods, E. F. Zganjar, B. Barmore, L. Gr. Ixaru, A. T. Kruppa, W. Nazarewicz, M. Rizea, T. Vertse, *Phys. Rev. C* **60**, (1999) 011301.
- [10] S. Aberg, P. B. Semmes, and W. Nazarewicz, *Phys. Rev. C* **56**, (1997) 1762 and *Phys. Rev. C* **58**, (1998) 3011.
- [11] W. B. Walters, in *PROCON99 - International Symposium on Proton-Emitting Nuclei*, edited by J. C. Batchelder, (AIP, New York, 2000) in press.
- [12] C. J. Gross, T. N. Ginter, D. Shapira, W. T. Milner, J. W. McConnell, A. N. James, J. W. Johnson, J. Mas, P. F. Mantica, R. L. Auble, J. J. Das, J. L. Blankenship, J. H. Hamilton, R. L. Robinson, Y. A. Akovali, C. Baktash, J. C. Batchelder, C. R. Bingham, M. J. Brinkman, H. K. Carter, R. A. Cunningham, T. Davinson, J. D. Fox, A. Galindo-Uribarri, R. Grzywacz, J. F. Liang, B. D. MacDonald, J. MacKenzie, S. D. Paul, A. Piechaczek, D. C. Radford, A. V. Ramayya, W. Reviol, D. Rudolph, K. Rykaczewski, K. S. Toth, W. Weintraub, C. Williams, P. J. Woods, C.-H. Yu, and E. F. Zganjar, *Nucl. Instrum. and Methods Phys. Res. Sect. A*, in press, and references therein.
- [13] T. M. Cormier, M. G. Herman, B. S. Lin, and P. M. Stwertka, *Nucl. Instrum. Methods* **212** (1983) 185.
- [14] E. F. Zganjar, A. Piechaczek, J. C. Batchelder, and C. J. Gross, in *Perspectives in Nuclear Physics*, edited by J. H. Hamilton, H. K. Carter, and R. B. Piercey, (World Scientific, Singapore, 1999) p. 187.
- [15] A. Piechaczek, A. Aprahamian, J. C. Batchelder, C. R. Bingham, D. Brenner, C. J. Gross, T. N. Ginter, R. Grzywacz, B. D. MacDonald, W. D. Kulp, S. D. Paul, J. J. Ressler, W. Reviol, K. Rykaczewski, R. Terry, K. S. Toth, W. B. Walters, J. A. Winger, J. L. Wood, and E. F. Zganjar, in *Perspectives in Nuclear Physics*, edited by J. H. Hamilton, H. K. Carter, and R. B. Piercey, (World Scientific, Singapore, 1999) p. 201.
- [16] J. Doering, H. Schatz, A. Aprahamian, R. C. de Haan, J. Gořres, M. Wiescher, W. B. Walters, J. Rikowska, L. T. Brown, C. N. Davids, C. J. Lister, D. Seweryniak, and B. Foy, *Phys. Rev. C* **57**, (1998) 1159.
- [17] P. J. Sellin, P. J. Woods, D. Branford, T. Davinson, N. J. Davis, D. G. Ireland, K. Livingston, R. D. Page, A. C. Shotter, S. Hofmann, R. A. Hunt, A. N. James, M. A. C. Hotchkis, M. A. Freer, and S. L. Thomas, *Nucl. Instrum. Methods A* **311**, (1992) 217.
- [18] S. L. Thomas, T. Davinson, and A. C. Shotter, *Nucl. Instrum. Methods in Phys. Res.* **A288**, (1990) 212.
- [19] T. Davinson, A. C. Shotter, E. W. MacDonald, P. Jobanputra, A. J. Stephens, and S. L. Thomas, *Nucl. Instrum. Methods in Phys. Res.* **A288**, (1990) 245.
- [20] K. Livingston, P. J. Woods, T. Davinson, N. J. Davis, S. Hofmann, A. N. James, R. D. Page, P. J. Sellin, and A. C. Shotter, *Phys. Lett.* **312B** (1993) 46.
- [21] K. S. Vierinen, J. M. Nitschke, P. A. Wilmarth, R. M. Chasteler, A. A. Shihab-Eldin, R. B. Firestone, K. S. Toth, and Y. A. Akovali, *Phys. Rev. C* **39**, (1989) 1972.

## V. TABLES

TABLE I. Summary of the measured proton energy and half-lives in the present experiment and the WKB proton partial half-life estimates as a function of angular momentum  $l$ . All half-lives are given in milliseconds and have large errors.

$E_p$ (MeV)	$T_{\frac{1}{2}}$	Isotope	$l=0$	$l=2$	$l=5$
0.885(15)	~100	$^{146}\text{Tm}$	31	263	$1.1 \times 10^6$
0.935(10)	~100	$^{146}\text{Tm}$	4.7	38	$1.6 \times 10^5$
1.032(10)	~200	$^{146}\text{Tm}$	0.18	1.5	$5.8 \times 10^3$
1.120(5)	~200	$^{146}\text{Tm}$	0.014	0.114	421
1.191(7)	~100	$^{146}\text{Tm}$	0.002	0.017	62
1.051(7)	~500	$^{147}\text{Tm}$	0.099	0.824	$3.1 \times 10^3$

## VI. FIGURES

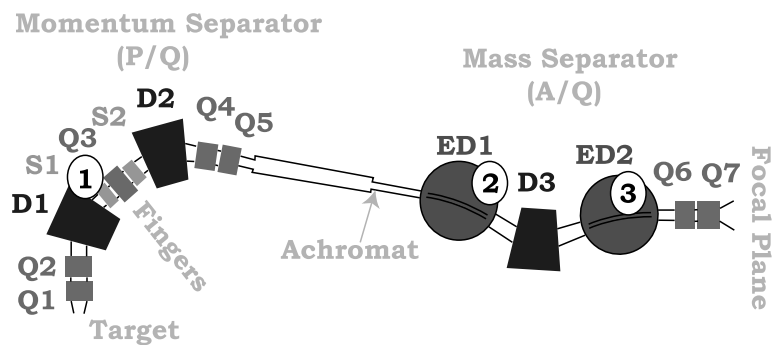


FIG. 1. A schematic view of the RMS. Areas (1) and (3) are the places where the primary beam is usually deposited inside the RMS. Areas (2) and (3) are places where the beam is deposited in similar mass spectrometers which do not have a momentum separator. The RMS achieves superior beam rejection by moving the first beam dump away from the final focal plane.

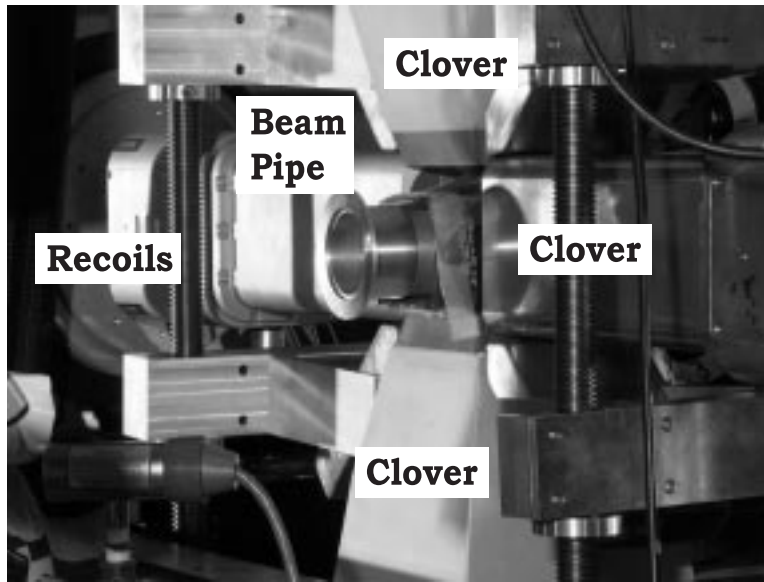


FIG. 2. A photograph of a typical experimental setup which uses the Moving Tape Collector (not shown). The close geometry of the Clover Ge detectors may be observed. Recoils are moved to the center of the setup by the moving tape which is inside the vacuum system.

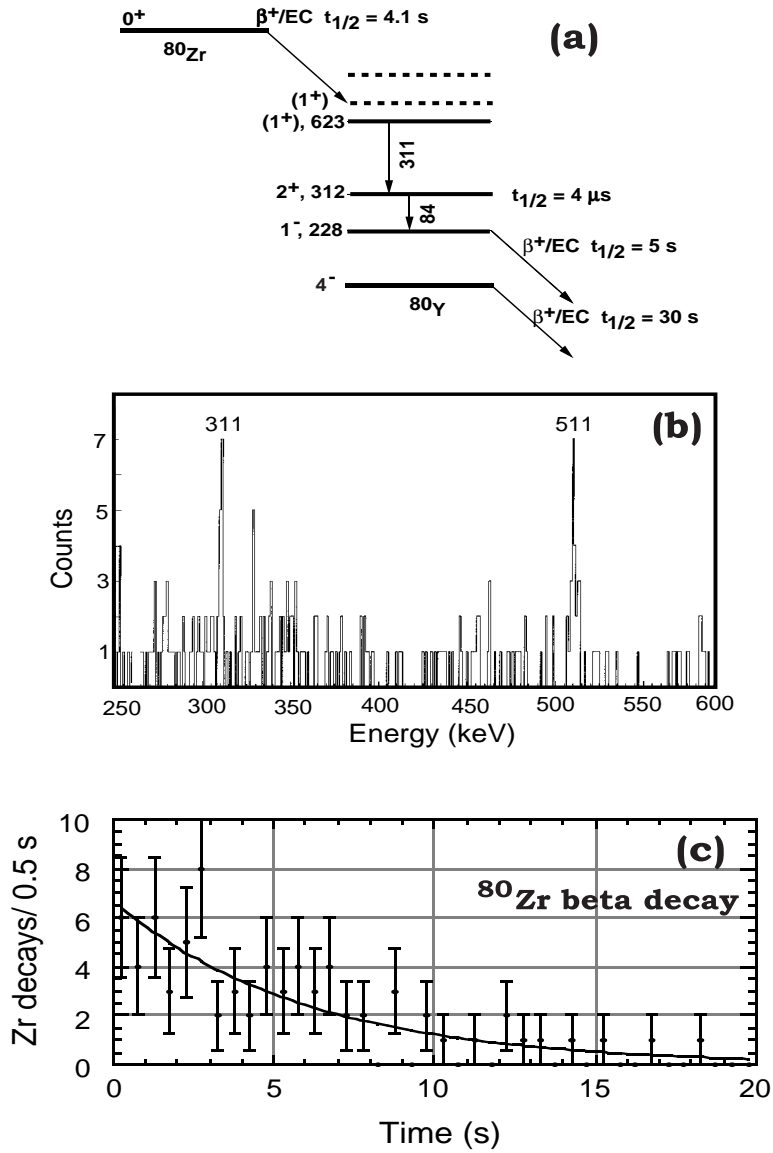


FIG. 3. (a) Partial decay scheme for  $^{80}\text{Zr} \rightarrow ^{80}\text{Y}$ . The feeding to the  $4$   $\mu\text{s}$  isomer allows a unique tag of  $^{80}\text{Zr}$  with little background from prompt decay. (b) Spectrum gated by the  $84$  keV  $\gamma$  ray which depopulates the isomer. The  $311$  keV transition and the  $511$  keV  $e^+e^-$  annihilation peak are clearly observed. (c) Decay rate data taken in the present work. The solid line represents the measured  $4.1$  s half-life. Figure taken from ref. [5].

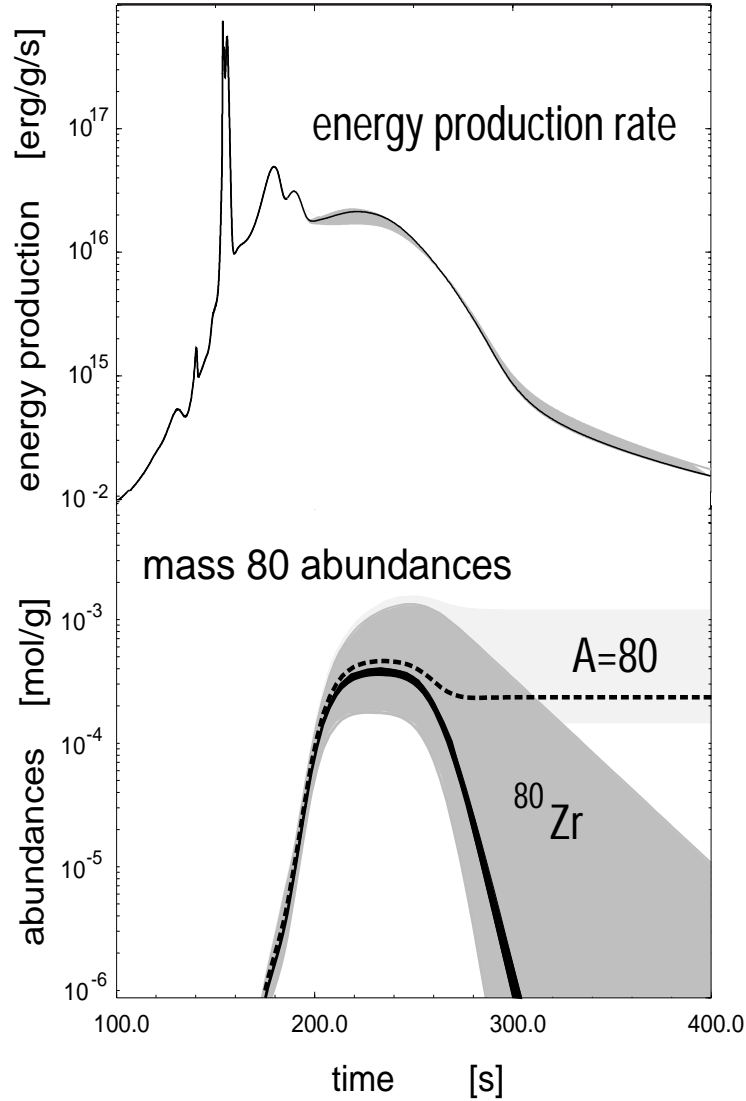


FIG. 4. The total energy production rate (upper) and the mass 80 abundances (lower) calculated in the present work. The shaded areas reflect the range of values when using various predicted half-lives (2.0 – 20 s) of  $^{80}\text{Zr}$ . The present measurement constrains the values to the solid ( $^{80}\text{Zr}$ ) and dashed lines (all isobars). The total energy production rate is not significantly impacted. Figure taken from ref. [5].

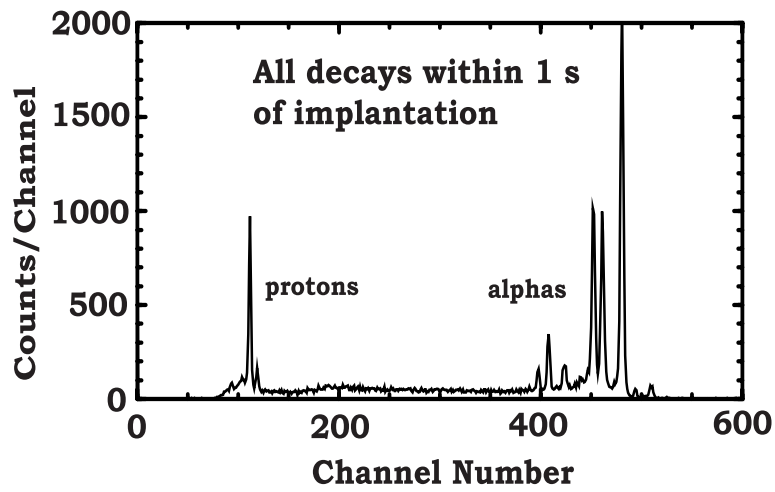
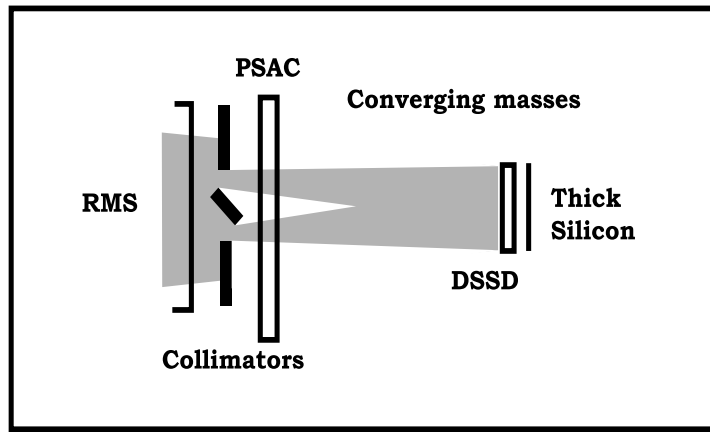


FIG. 5. (Top) The schematic view of the experimental setup. (Bottom) The total decay spectrum 1 s after implantation. The higher energy peaks are due to alpha decays from contaminant reactions due to target impurities.

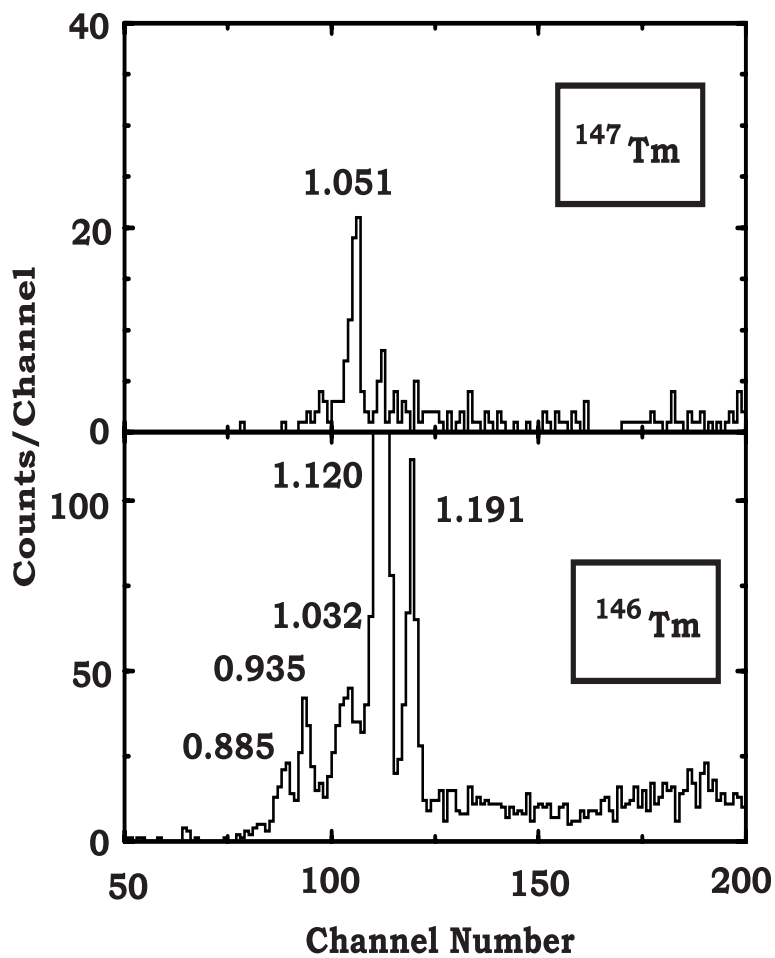


FIG. 6. The proton decay spectrum for  $^{147}\text{Tm}$  and  $^{146}\text{Tm}$  within 200 ms of implantation. The energies are in MeV. The data are from all runs with and without absorbers. The peak at 1.120 MeV extends beyond the range shown.

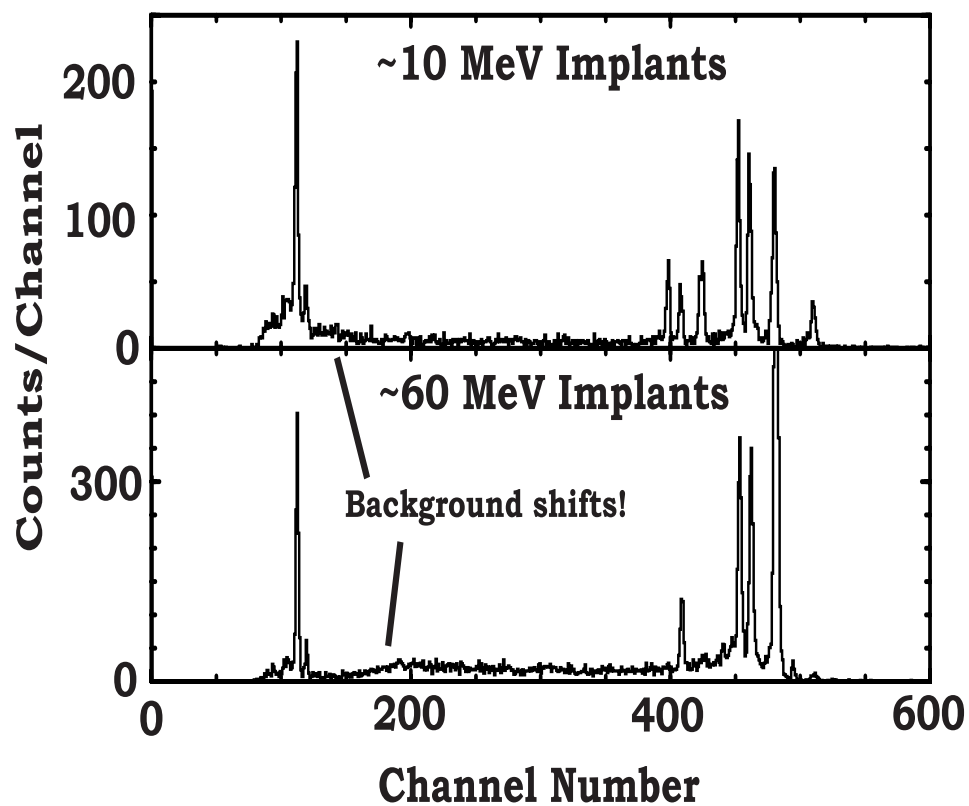


FIG. 7. The decay spectra taken with and without absorbers within 500 ms of implantation. The approximate implantation energy is given. Note the shift of the background to higher energies in the bottom spectrum. The background is caused by decays escaping the detector and depositing only a fraction of their energy.

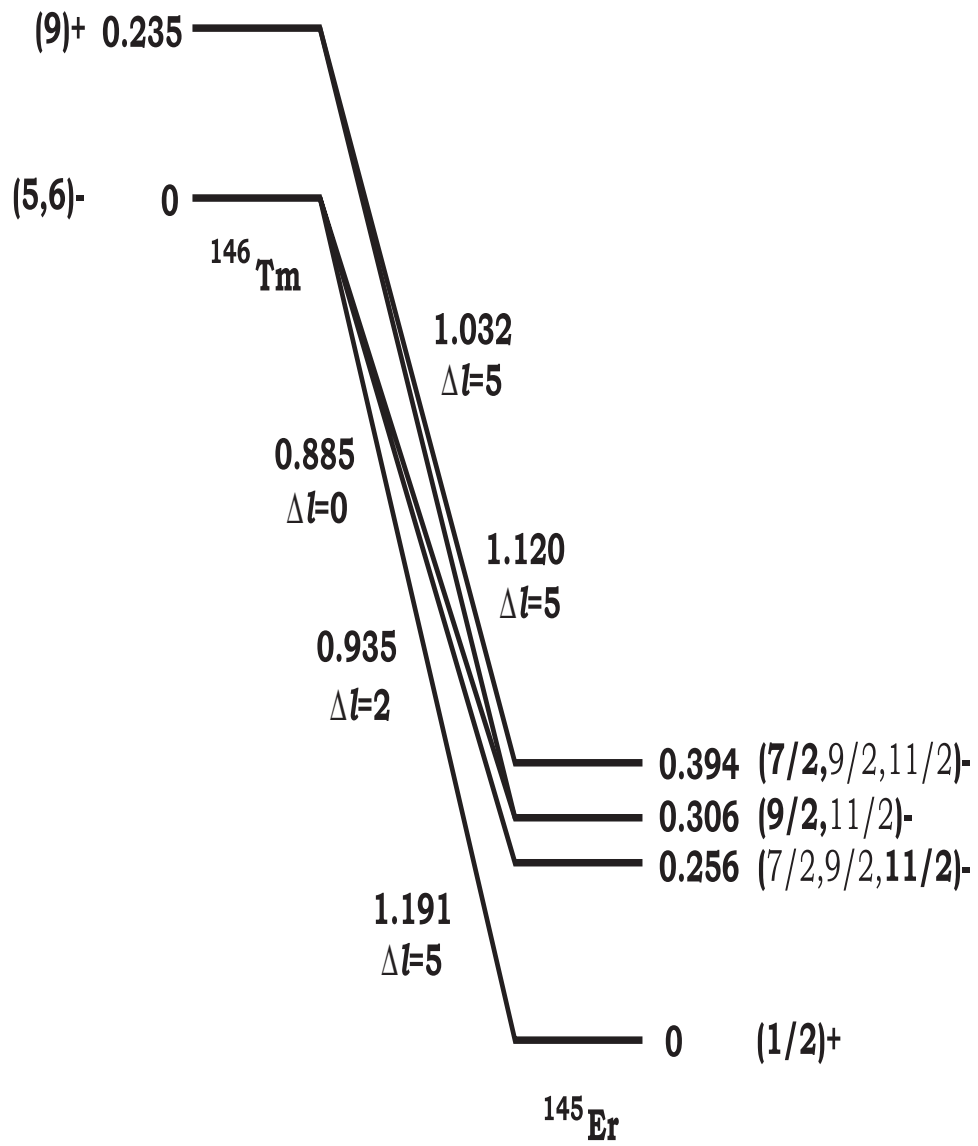


FIG. 8. The decay level scheme for proton emission from  $^{146}\text{Tm}$ . All energies are given in MeV.